Tribology Online

Japanese Society of Tribologists

http://www.tribology.jp/trol/

Vol. 14, No. 5 (2019) 367-374.
ISSN 1881-2198
DOI 10.2474/trol.14.367

Article

A Combined Experimental and Theoretical Study on the Mechanisms Behind Tribocharging Phenomenon and the Influence of Triboemission

Alessandra Ciniero[1, 2)*], Giulio Fatti[1)], Maria Clelia Righi[1, 3)], Daniele Dini[2)] and Tom Reddyhoff[2)]

[1)] Department of Physics, Informatics and Mathematics, University of Modena and Reggio Emilia, Via Campi, 213/A 41125 Modena, Italy
[2)] Tribology Group, Department of Mechanical Engineering, Imperial College London, London SW7 2AZ, UK
[3)] CNR-Institute of Nanoscience, S3 Center, Via Campi 213/A, 41125 Modena, Italy

*Corresponding author: Alessandra Ciniero (aciniero@unimore.it)

Manuscript received 03 July 2019; accepted 12 September 2019; published 15 December 2019
Presented at the International Tribology Conference Sendai 2019, 17-21 September, 2019

Abstract

This work describes recent research into the mechanisms behind tribocharging and the influence of triboemission. The term tribocharging is a type of contact-induced electrification and refers to the transfer of charge between rubbing components. The term triboemission, on the other hand, refers to emission of electrons, ions and photons generated when surfaces are rubbed together. The understanding of tribocharging is of wide interest for several industrial applications and in particular the combination of tribocharging and triboemission may be important in lubricated contacts in the formation of boundary lubricant films. We report the use of a unique vacuum measurement system that enables to measure surface charge variations while simultaneously recording triboemission events during the sliding of a diamond tip on silica specimens. Results show for the first time that tribocharging and triboemission behavior are linked and depend on the surface wear. The contribution of contact-induced electrification to the charging of the surface is then described by means of density functional theory (DFT). Results give insight into the transfer of charge from the SiO_2 amorphous surface (silica) to the C(111) surface (diamond) and into the variation of charging during simulated sliding contact.

Keywords

tribocharging, triboemission, silica amorphous, diamond, DFT

1 Introduction

The term tribocharging refers to the transfer of charge between rubbing components. A wide range of factors influences the transfer and the generation of charge, at macroscopic and atomic level. For instance, material stress can cause bond scission that results in a rearrangement of the charge of the surface and the release of ions and electrons [1]. The importance of tribocharging has led to the development of new nanoscale techniques and theoretical analysis [2] to study this phenomenon and to better understand its fundamental mechanisms. In industry, tribocharging is employed in many applications including sliding [3] and dry bearings [4], pharmaceutical [5, 6], space [7] and green energy harvesting [8, 9] and it has the potential to be at the forefront of technological innovations. In particular, in lubricated contacts in the formation of boundary films and in certain cases in their degradation tribocharging and a phenomenon known collectively as triboemission they have been suggested as playing a key role. Triboemission consists of emission of charged particles such as electrons, protons, positive and negative ions and also acoustic emission that occur when hard, solid surfaces are rubbed together [10-17]. If a lubricant is present, these particles may promote chemical reactions that lead to both degradation [18], and formation of protective films on the surface of components [19]. Previous studies, on tribocharging effects, have shown the occurring of various tribochemical reactions during wear due to contact potential differences on the worn surfaces [20]. It has been found that the electrical potential of the materials can differ due to tribologically generated phase transformed regions and that nanoscale wear causes chemical and structural changes to the material surfaces [21, 22]. Under lubricated conditions the voltage of the surface induced by frictional contact was found dependent on the movement of charge and influencing the friction and the type of wear [23-25]. Other studies have reported the influence of combination of tribocharging and triboemission in both dry and lubricated contacts [26-28]. These studies showed that lubricating oil molecules are excited and decomposed by the emission of electrons accelerated by the tribocharging-electric filed both inside and outside of the sliding contact.

Copyright © 2019 Japanese Society of Tribologists
This article is distributed under the terms of the latest version of CC BY-NC-ND defined by the Creative Commons Attribution License.

Despite years of research these two phenomena are not yet well understood because of the limits of experimental techniques at atomic level and because of lack of theoretical studies. This study aimed at elucidating the underlying mechanisms of tribocharging and triboemission by combing experimental and theoretical methods. A recently developed measurement system is used to obtain information of the charging of the silica and emission events during the sliding of a simulate asperity contact. A theoretical approach based on first-principles methods is, instead, used to provide insights into the contribution of contact-induced electrification to the charging of the surface.

2 Research methods

2.1 Experimental method

The experimental part of this study was conducted by using a unique high vacuum in-house built tribometer [12, 13, 29], schematically represented in Fig. 1. It consists of: i) a system of microchannel plates (MCPs, i.e. arrays of electrons multipliers), coupled with a phosphor screen to detect and visualize the emission, respectively; ii) a loading system comprising of a dead-weight arrangement and a diamond tip of radius 100 μm to produce the sliding contact; iii) and a PCS Instruments encoder device used to record the rotation of the disc. A high-speed camera located above the experimental setup was used to record the emission as they appeared on the phosphor screen. In addition, simultaneously with the emission detection, an electrometer coupled with a 10 × 5 mm metal sheet electrode attached underneath the specimen was used to inductively measure the accumulation of the charge on the specimens.

The tests were conducted in vacuum conditions at a pressure of ~10^{-3} Pa. The detection of negative particles (i.e. 10–85% of 0.01–50 keV [30]) was obtained by applying 1.5 kV, and 5 kV to the input MCP and output MCP, respectively, with the phosphor screen being grounded. A sliding velocity of 50 mm/s and a load of 0.5 N were set for all the tests. The encoder, the frame rate of the high speed camera and the electrometer acquisition were synchronized at 125 Hz. The specimens used were silica amorphous discs (diameter of 46 mm and a thickness of 6 mm). Prior to each test the discs were cleaned with toluene followed by isopropanol in an ultrasonic bath (15 minutes for each chemical). The surface analysis of each specimen was conducted by using the Veeco Wyco NT9100 optical profiler.

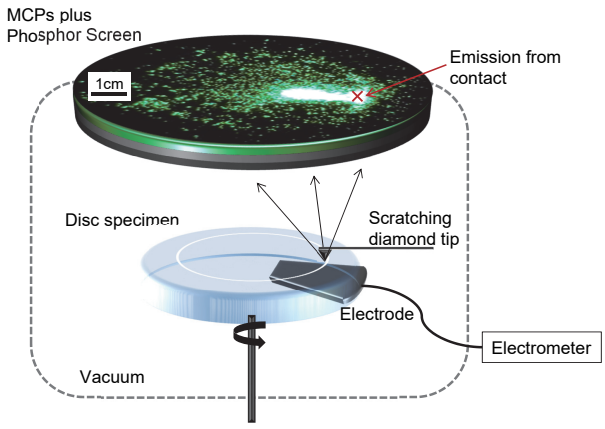

Fig. 1 Schematic of the high vacuum tribometer

2.2 Computational method

The theoretical part of this study was conducted by employing first-principles calculations based on Density Functional Theory (DFT) as implemented in the Quantum ESPRESSO package to describe the transfer of the electrons between silica and diamond. We adopted local density approximation (LDA) as parameterized by Perdew-Zunger (PZ) to describe the exchange-correlation term [31]. The kinetic energy cut-off of the plane wave expansion was set to 35 Ry. An orthorhombic cell of 9.83 × 17.03 × 35.00 Å dimensions including a vacuum region of 10 Å and gamma-point centered Monkhorst–Pack k-point grid [32] was used in all the calculations. The dimension of the system can be considered big enough to take in account the silica amorphous correlation length (4 – 8 Å [33]) and to mimic bulklike features of the respective slabs.

The silica bulk was prepared by classical MD in a periodic 9.83 × 17.03 × 10.79 Å cell with 48 O and 96 Si atoms. The variable-charge interatomic potentials used for the classical MD simulation are the charge-optimized many-body (COMB) potential for Si/SiO_2 [34] as implemented in the Large-scale Atomic/Molecular Massively Parallel Simulator (LAMMPS) software [35]. The initial α-quartz structure was heated from 300K to 3000K for 100ps at a constant temperature and pressure allowing the shape and the size of the simulation box to change. The silica melt was then maintained at 3000K at a constant box volume for 100ps to ensure a complete melting. The silica melt was then quenched at 300K for 100ps [36]. The final density and cohesive energy of the amorphous silica thus obtained are 2.36 g/cm^3 and -19.22 eV in agreement with experimental measurements [37]. The average values of Si-O and O-O bond length and O-Si-O bond angle obtained are 1.57 Å, 2.71 Å and 106.5°, respectively. These are in agreement with experimental values of 1.6 Å, 2.6 Å and 109.28° [38].

The diamond slab was constructed from (4 × 7)-C(111) surface, with the vacuum side Pandey reconstructed, resulting in a slab of 320 carbon atoms distributed on five bi-layers, corresponding to a thickness of 8.77 Å. This geometry consists of planar zig-zag carbon chains extended at different quotas. The outermost chain displays C-C length of 1.44 Å, instead the lower chain is characterized by C-C bond length of 1.5 Å, corresponding to that associated with sp^3 coordination [39]. While the other horizontal C-C bonds have same length (in consistency with the literature which reported no dimerization on the chains [40-42]), the C-C bonds below the top bilayer are characterized by an alternation of shorter and longer length. The Pandey reconstruction was chosen because of its most stable termination not only of the (111) surface but also of all the low-index diamond surfaces. At the interface, instead, the diamond slab was cut perpendicular to the [111] direction, generating unreconstructed C(111) surface, allowing the carbon atom dangling bonds to interact with the silica surface. The size of the diamond slab was chosen in order to minimize the mismatch with the silica.

The two slabs were placed together at a distance of ~2 Å with the silica amorphous slab at the bottom and the C(111) slab above as shown in Fig. 2, the atoms were allowed to relax to achieve the equilibrium configuration which resulted in a total slab height of 22.25 Å.

In order to simulate the variation of the distance between the two surfaces that occurs during sliding the two slabs were separated by moving the upper slab in discrete steps along the z direction and letting the system to relax after each step [43]. For

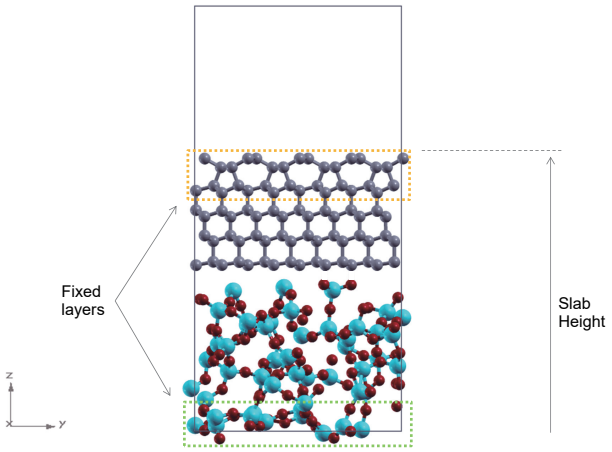

Fig. 2 Orthorhombic cell, (4 × 7)-C(111) Pandey reconstructed slab (top) and amorphous SiO_2 slab (bottom)

the atomic relaxations the top two bi-layers of the C(111) and the SiO_2 atoms up to 3.45 Å in the z direction were kept fixed at bulklike distance, whereas the intermediate atoms were allowed to fully relax. The separation of the slabs was initiated from the equilibrium and to simulate a realistic separation only the topmost rigid C(111) layers were moved in discrete steps of 0.1 Å in the positive z direction.

3 Results and discussion

3.1 Experimental outcomes

3.1.1 Charge and emission measurement during sliding test without fracture

Sliding tests where no fractures were observed on the surface (an example is shown in Fig. 5 (d)) generate positive charge of the surface and low negative emission. The cumulative value of the charge of the surface and the cumulative value of the average intensity of each phosphor screen image are plotted as function of the time in Fig. 3 (a).

The surface charge measurements and the simultaneously average of emission intensity show a correlation between charging and emission. It can be seen that the silica charges positively in accordance with the triboelectric series [44-46] and previous studies [47-49] while the intensity of the emission increases over time. Observations of the resulting linearity of surface charge and the emission intensity curve leads to the conclusion that the emission of negatively charged particles contributes to the positive charging of the silica specimen.

The discretization of both charge and emission measurements is presented in Fig. 3 (b). This shows that both the charge and the emission intensity are characterized by numerous high peaks which begin to occur simultaneously at the start of the sliding. These results support the theory that emission is due to the wearing of the surface as previously observed [50-53, 28] and that in turn the wear influences the charge of the surface. A clear correlation between the charge and the average emission intensity is evident when observing the zoomed in Fig. 3 (c).

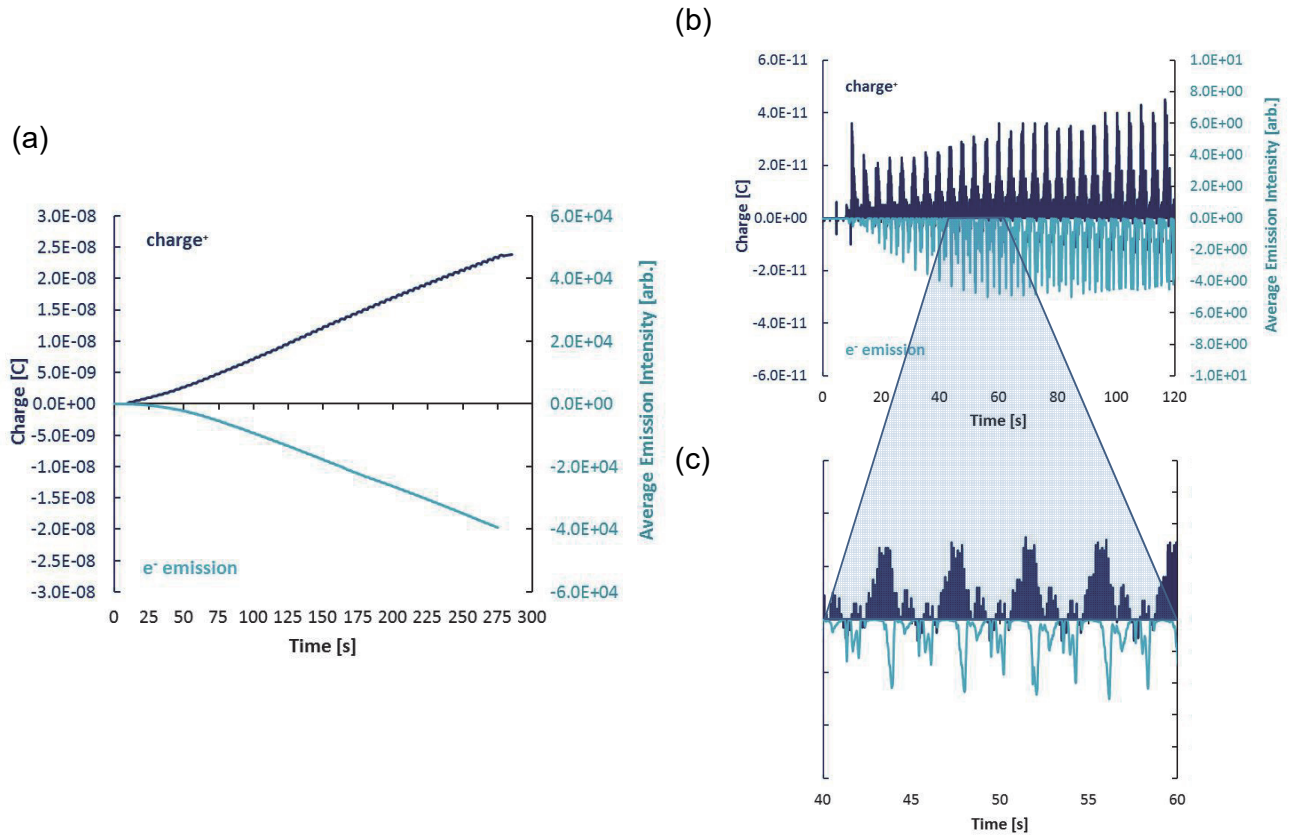

Fig. 3 (a) Average intensity of each phosphor screen image and surface charge vs. time (cumulative values); (b) Average intensity of each phosphor screen image and surface charge vs. time, (instantaneous values), (c) Zoom of the period between 40 s and 60 s, during sliding test without fracture

Here, a correspondence can be seen between peaks of positive charges and peaks of negative emission. This again suggests that negative particles leaving the specimen result in an increase of positive charge on its surface. The periodic repetition of the charge signal and its negative peaks may be caused by the non-uniformity of the surface due to wear and by the fact that the glass specimens used in these experiments were not made from a uniform single crystal but were instead amorphous materials containing random defects [54, 55]. These charge measurements agree well with recent studies about the non-uniformity of the charge of the surface during contact [56], the transfer and re-transfer of electrons and the transfer of material between the surfaces in contact [1, 57].

3.1.2 Charge and emission measurement during sliding test with fracture

In tests when fractures were observed on the sliding surface, the comparison between surface charge and the average intensity of the emission reveals a different trend. Figure 4 (a) shows the accumulation of charge on the surface and the cumulative average emission intensity of each phosphor screen images as a function of time.

Initially, as expected, the surface charges positively due to the emission of negative particles. However, in the period between ~80 s and ~100 s, the sudden increase of the emission results in the abrupt drop of the charge suggesting an inversion of the surface charging.

When comparing the instantaneous values of the charge of the surface with the instantaneous values of the emission intensity during fracture (Fig. 4 (c)) a correspondence between peaks of negative charge and peaks of negative emission can be noticed. This suggests that, unlike the case of sliding without fractures, even if significant negative emission is detected, the particles escaping the surface during fracture are mainly positively charged. This causes the negative charging of the silica surface, in contrast with the triboelectric series predictions.

To analyse the cause of this unexpected change of emission intensity, the phosphor screen images were evaluated. During the highlighted period of Fig. 4, the phosphor screen revealed emission events of different intensity, shape and size compare to the emission events recorded at the beginning (Fig. 5 (a)) and at the end (Fig. 5 (c)) of the test. An example of these images is shown in (Fig. 5 (b)). The events are brighter and extensive. The subsequent scans of the surface, an example of which is reported in (Fig. 5 (e)) showed fractures at the areas where this type of emission was detected, suggesting that high emission intensity events occur at the moment when the tip causes fracture of the surface.

The analysis of the wear track in case of fracture reports an average depth and width of 14 μm and 89.87 μm, respectively which is, indeed, significantly higher than the depth and width of the wear track in case of sliding without fracture (~0.19 μm and ~36 μm, respectively).

The experimental outcomes show that the emission of negative particles due to the rubbing contributes to the positive charging of the silica specimen. Conversely, during the occurrence of fracture, the emission generated causes the silica to charge more negatively, suggesting that this emission consists mainly of positive particles. Overall, it can be suggested that both tribocharging and triboemission are influenced by the

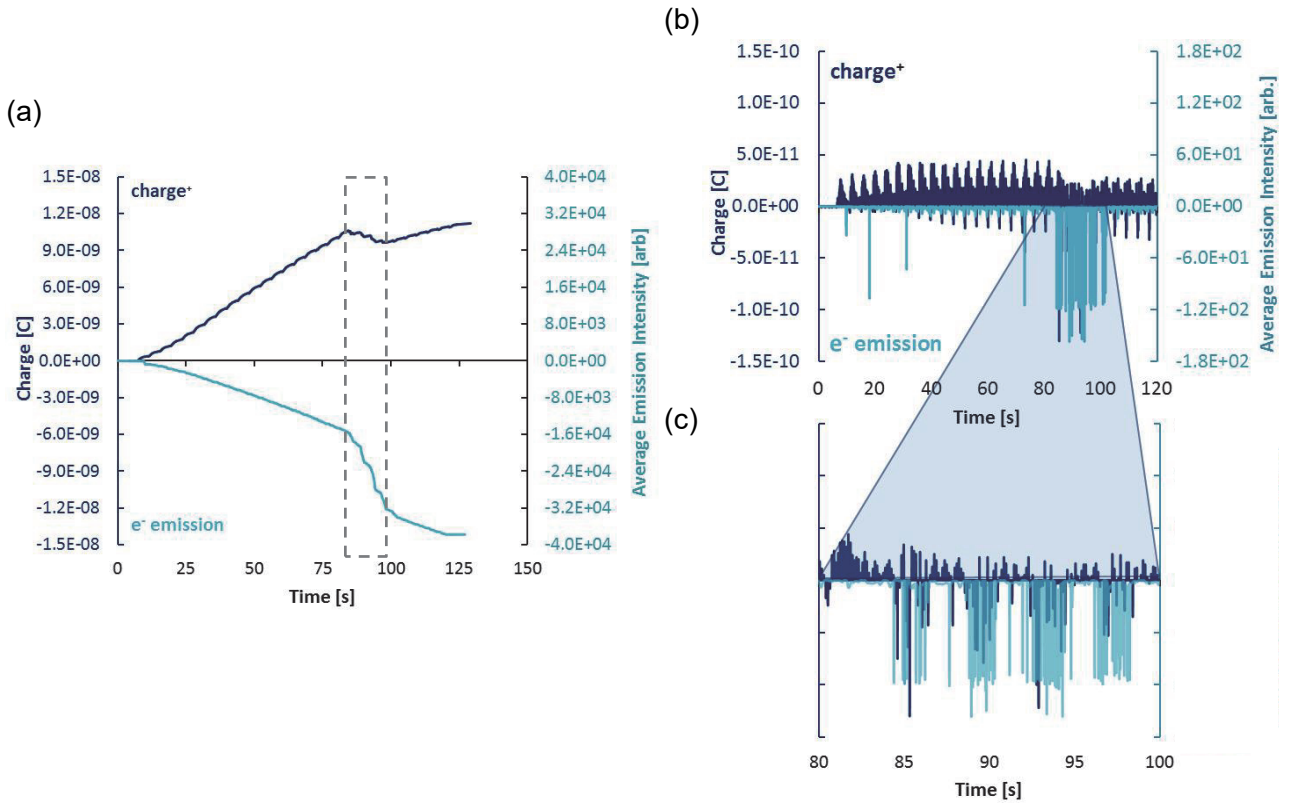

Fig. 4 (a) Average intensity of each phosphor screen image and surface charge vs. time (cumulative values); (b) Average intensity of each phosphor screen image and surface charge vs. time (instantaneous values), (c) Zoom of the period between 80 s and 100 s, during sliding test with fracture

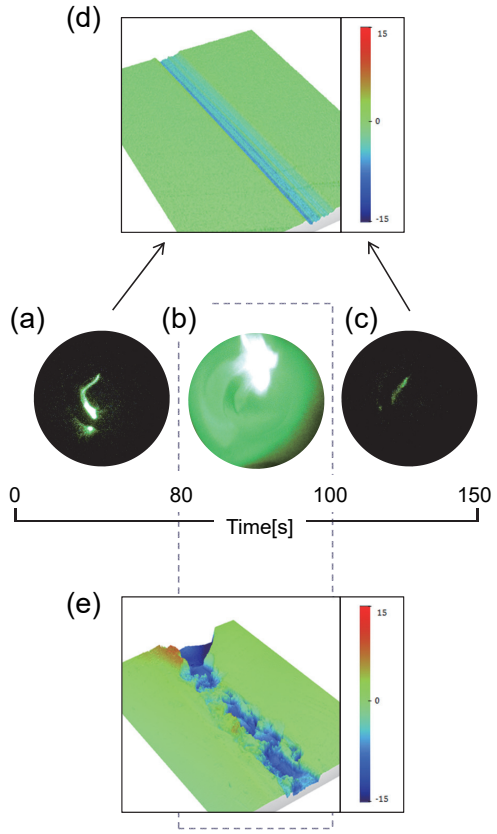

Fig. 5 Triboemission events (a) at the beginning, (b) during fracture and (c) at the end of the test; White Light Interferometry (WLI) scan of the surface at (d) rubbing area (e) at fracture area

wear and that the emission of charged particles influences the charging of the surface.

3.2 Theoretical outcomes

In both the experimental tests reported above silica specimens have been subjected to conduct-induced electrification. The contribution of this is here investigated theoretically by examining the difference of charge density at the interface. This is calculated via

$$\rho_{diff} = \rho_{C(111)/SiO_2} - (\rho_{C(111)} + \rho_{SiO_2})$$

where $\rho_{C(111)/SiO_2}$ is the charge density of the interface and $\rho_{C(111)}$ and ρ_{SiO_2} are the charge density of the isolated slabs. Figures 6 (a) and (b) show such charge-density differences at the interface between C(111) and amorphous SiO_2, respectively. It can be noticed a significant electron charge accumulation at the C(111) side of the interface which results in a loss of electron charge at amorphous SiO_2 interface side. To observe how the charge is displaced across the interface, the charge-density difference is integrated in the *xy planar* dimensions. The resulting $\rho_{diff}(z) = \int \rho_{diff}\, dxdy$ along the z axis is shown in Fig. 6 (c) for a limited region around the interface, where the zero indicates the diamond surface. This shows a significant depletion at the silica interface side and a transfer of charge towards the diamond slab.

This analysis supports the outcomes of the sliding test reported in the previous sections. In particular, it confirms that, also at atomic level, silica loses electrons, i.e. charges positively, when in contact with diamond. Moreover, it gives insights into the electronic properties of contact-induced electrification.

The influence of the sliding to the charge transfer was simulated by separating the two slabs using discrete steps of 0.1 Å, starting from the equilibrium configuration. The comparison of the integrated charge density difference at the interface between three different slab heights (22.25 Å (equilibrium),

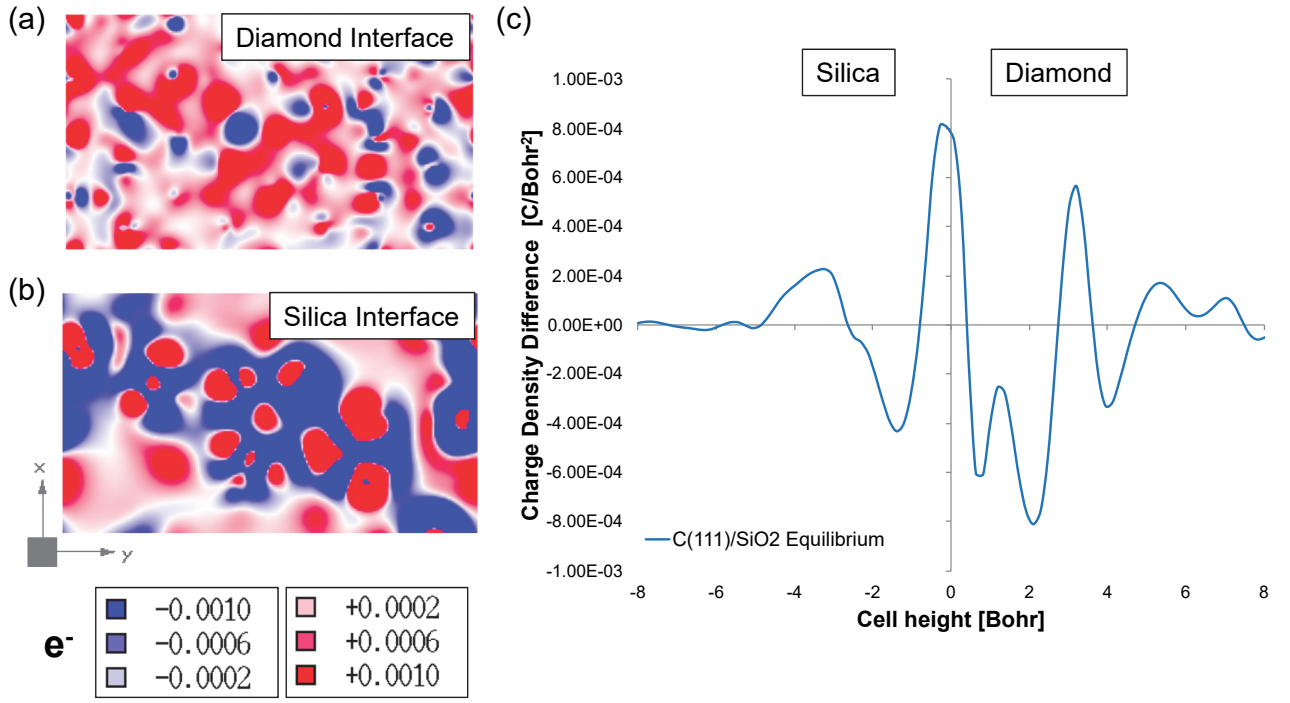

Fig. 6 Charge density difference isosurfaces at (a) C(111) interface and at (b) amorphous SiO_2 interface; (c) Integrated charge-density difference along cell height

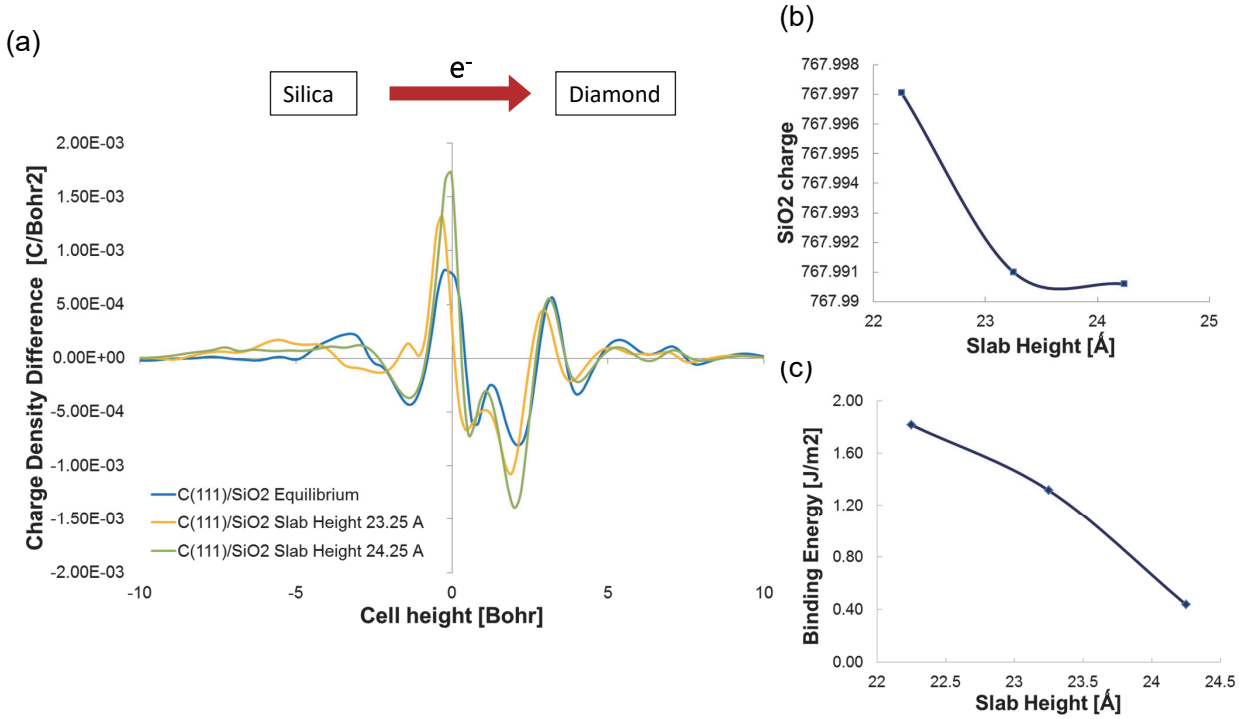

Fig. 7 (a) Integrated charge-density difference along the cell height for free different slab heights; (b) Bader charge measurements of SiO_2 slab vs slab height; (c) Binding energy between C(111) slab and SiO_2 slab vs slab height

23.25 Å and 24.25 Å), the total charge of the silica slab and the binding energy between the C(111) slab and SiO_2 slab during the separation are reported in figure a, b, c, respectively.

The comparison of the charge density difference (Fig. 7 (a)) shows that the separation of the C(111) slab from the amorphous SiO_2 slab results in an higher transfer of electrons from the silica slab to the diamond slab compare to the equilibrium configuration. In support of this, the calculation of the Bader charges [58, 59] of the SiO_2 slab reports a decrease of the total charge with the increase of slab height (Fig. 7 (b)). This is in agreement with the experimental outcomes which show an accumulation of positive charge on silica specimens over the time.

The evaluation of the binding energy between the two slabs shows a decrease of energy with the increment of the slab height (Fig. 7 (c)). This is consistent with the analysis of the bond lengths of the atoms at the interface which reports a significant stretch compare to the equilibrium configuration. On average, Si-O bond length in the last step is of about 1.86 Å, thus 0.18 Å longer than the bond length at the equilibrium; instead C-C bond length is of about 1.65 Å, 0.08 Å longer than the equilibrium length. Also for the C-Si and C-O bond a stretch of 0.38 Å and 0.04 Å is calculated, respectively. The elongation of the Si-O and C-Si bonds favors the transfer of the charge from the C(111) slab to the SiO_2 slab, which is in agreement with the charge density difference shown in Fig. 7 (a).

The reduction of the binding energy and the stretching of the bond lengths might also promote the escape of some of the electrons located at the interface. Moreover, the significant elongation of the Si-O bond lengths suggests a probable break of the bonds and a consequent removal of silica layers from the silica slab. This will give addition information about the mechanism behind tribocharging, in particular about the role of material transfer and how this affects the charge of the surface.

4 Conclusions

The study here reported gives insight into the mechanisms behind tribocharging. Results of the influence of the emission of charged particle due to the rubbing and results of the influence of contact-induced electrification are obtained by a combined experimental and theoretical approach. Sliding tests on silica specimens rubbed with a diamond tip carried out by using a unique in-house built tribometer, showed that silica specimens charge positively during the sliding in case no fractures occur. In particular, the linearity between the positive charging of the silica and the emission of negative charges showed that the silica charges more positively as more electrons leave the surface. Contrarily, if fracture occurs the surface charged negatively, suggesting the emission of positive charged particles. Overall, the experimental outcomes showed that the surface is subjected to a non-uniformity of the charging which is due to the type of wear and the structure of the material.

The contribution of the contact-induced electrification to the charging of the surface was evaluated by employing first-principles methods. The transfer of electron charge from the amorphous SiO_2 slab to the C(111) slab was clearly shown by the analysis of the charge density difference at the interface. The isosurfaces showed the accumulation of charge at the C(111) slab interface and the loss of charge at SiO_2 slab interface. The transfer charge analysis of the simulated sliding showed, in agreement with the experimental outcomes, an increase of the transfer of the charge from the SiO_2 slab to the C(111) slab with the increase of the slab height. This was supported by the Bader charge analysis which resulted in a reduction of the total charge of the silica slab, the reduction of the binding energy between the two slabs and the elongation at the interface of the Si-O and C-Si bond lengths. This last outcome, in particular, suggested the possibility of breaking of the bonds and material transfer

from the silica to the diamond surface.

This combined study shed a light on the understanding of the mechanisms behind tribocharging at macroscopic and atomic level. Moreover, the theoretical approach gives the possibility to gain additional information at the atomic level of a phenomenon that is of high interest for established industrial fields as well as for new advance technologies.

Acknowledgments

This research was supported by European Union Horizon 2020 Marie Curie Actions Grant Agreement No. 798245 for Dr Ciniero, the UK Engineering and Physical Research Sciences Research Council (EPSRC – Doctoral Fellowship Prize for Dr Ciniero and Prof. Dini's Established Career Fellowship EP/N025954/1) and the Taiho Kogyo Tribology Research Foundation (TTRF). Computational resources have been provided by the supercomputing facilities CINECA consortium and Imperial College London Research Computing Service (RCS).

References

[1] Burgo, T. A., Ducati, T. R. D., Francisco, K. R., Clinckspoor, K. J., Galembeck, F. and Galembeck, S. E., "Triboelectricity: Macroscopic Charge Patterns Formed by Self-Arraying Ions on Polymer Surfaces," Langmuir, 28, 19, 2012, 7407-7416.

[2] Fatti, G., Righi, M. C., Dini, D. and Ciniero, A., "First-Principles Insights into the Structural and Electronic Properties of Polytetrafluoroethylene in Its High-Pressure Phase (Form III)," The Journal of Physical Chemistry C, 123, 10, 2019, 6250-6255.

[3] Mokha, A., Constantinou, M. and Reinhorn, A., "Teflon Bearings in Base Isolation I: Testing," Journal of Structural Engineering, 116, 2, 1990, 438-454.

[4] Lancaster, J. K., "Accelerated Wear Testing of PTFE Composite Bearing Materials," Tribology International, 12, 2, 1979, 65-75.

[5] Pu, Y., Mazumder, M. and Cooney, C., "Effects of Electrostatic Charging on Pharmaceutical Powder Blending Homogeneity," Journal of Pharmaceutical Sciences, 98, 7, 2009, 2412-2421.

[6] Karner, S. and Urbanetz, N. A., "The Impact of Electrostatic Charge in Pharmaceutical Powders with Specific Focus on Inhalation-Powders," Journal of Aerosol Science, 42, 6, 2011, 428-445.

[7] Sinclair, P. C., "General Characteristics of Dust Devils," Journal of Applied Meteorology, 8, 1, 1969, 32-45.

[8] Wang, S., Lin, L. and Wang, Z. L., "Nanoscale Triboelectric-Effect-Enabled Energy Conversion for Sustainably Powering Portable Electronics," Nano Letters, 12, 12, 2012, 6339-6346.

[9] Su, Y., Chen, J., Wu, Z. and Jiang, Y., "Low Temperature Dependence of Triboelectric Effect for Energy Harvesting and Self-Powered Active Sensing," Applied Physics Letters, 106, 1, 2015, 013114.

[10] Nakayama, K. and Hashimoto, H., "Triboemission from Various Materials in Atmosphere," Wear, 147, 2, 1991, 335-343.

[11] Nakayama, K., "Triboemission of Charged Particles and Resistivity of Solids," Tribology Letters, 6, 1, 1999, 37-40.

[12] Dickinson, J. T., Donaldson, E. E. and Park, M. K., "The Emission of Electrons and Positive Ions from Fracture of Materials," Journal of Materials Science, 16, 10, 1981, 2897-2908.

[13] Dickinson, J. T., Snyder, D. B. and Donaldson, E. E., "Electron and Acoustic Emission Accompanying Oxide Coating Fracture," Thin Solid Films, 72, 2, 1980, 223-228.

[14] Ciniero, A., Le Rouzic, J. and Reddyhoff, T., "The Use of Triboemission Imaging and Charge Measurements to Study DLC Coating Failure," Coatings, 7, 8, 2017, 129.

[15] Ciniero, A., Le Rouzic, J. L., Baikie, I. and Reddyhoff, T., "The Origins of Triboemission -- Correlating Wear Damage with Electron Emission," Wear, 374-375, 2017, 113-119.

[16] Ciniero, A., "Triboemission Mechanisms," Imperial College London, 2017.

[17] Ciniero, A., Dini, D. and Reddyhoff, T., "An Experimental and Theoretical Approach to Study the Link between Triboemission and Tribocharging," APS Meeting Abstracts, 2018.

[18] Zhao, X. and Bhushan, B., "Studies on Degradation Mechanisms of Lubricants for Magnetic Thin-Film Rigid Disks," Proceedings of the Institution of Mechanical Engineers, Part J: Journal of Engineering Tribology, 215, 2, 2001, 173-188.

[19] Spikes, H., "The History and Mechanisms of ZDDP," Tribology Letters, 17, 3, 2004, 469-489.

[20] Kasai, T., Fu, X. Y., Rigney, D. A. and Zharin, A. L., "Applications of a Non-Contacting Kelvin Probe during Sliding," Wear, 225-229, 1999, 1186-1204.

[21] DeVecchio, D. and Bhushan, B., "Use of a Nanoscale Kelvin Probe for Detecting Wear Precursors," Review of Scientific Instruments, 69, 10, 1998, 3618-3624.

[22] Zharin, A. L. and Rigney, D. A., "Application of the Contact Potential Difference Technique for On-Line Rubbing Surface Monitoring," Tribology Letters, 4, 2, 1998, 205-213.

[23] Goto, K., "The Influence of Surface Induced Voltage on the Wear Mode of Stainless Steel," Wear, 185, 1-2, 1995, 75-81.

[24] Brandon, N. P., Bonanos, N., Fogarty, P. O., Mahmood, M. N., Moore, A. J. and Wood, R. J. K., "Influence of Potential on the Friction and Wear of Mild Steel in a Model Aqueous Lubricant," Journal of Applied Electrochemistry, 23, 5, 1993, 456-462.

[25] Brandon, N. P. and Wood, R. J. K., "The Influence of Interfacial Potential on Friction and Wear in an Aqueous Drilling Mud," Wear, 170, 1, 1993, 33-38.

[26] Nakayama, K., Suzuki, N. and Hashimoto, H., "Triboemission of Charged Particles and Photons from Solid Surfaces during Frictional Damage," Journal of Physics D: Applied Physics, 25, 2, 1992, 303.

[27] Nakayama, K., "Triboemission of Electrons, Ions, and Photons from Diamondlike Carbon Films and Generation of Tribomicroplasma," Surface and Coatings Technology, 188–189, 2004, 599-604.

[28] Nakayama, K., Leiva, J. A. and Enomoto, Y., "Chemi-Emission of Electrons from Metal Surfaces in the Cutting Process due to Metal/Gas Interactions," Tribology International, 28, 8, 1995, 507-515.

[29] Le Rouzic, J. and Reddyhoff, T., "Spatially Resolved Triboemission Measurements," Tribology Letters, 55, 2, 2014, 245-252.

[30] Wiza, J. L., "Microchannel Plate Detectors," Nuclear Instruments and Methods, 162, 1, 1979, 587-601.

[31] Perdew, J. P. and Zunger, A., "Self-Interaction Correction to Density-Functional Approximations for Many-Electron Systems," Physical Review B, 23, 10, 1981, 5048.

[32] Monkhorst, H. J. and Pack, J. D., "Special Points for Brillouin-Zone Integrations," Physical Review B, 13, 12, 1976, 5188.

[33] Susman, S., Volin, K. J., Price, D. L., Grimsditch, M., Rino, J. P., Kalia, R. K., Vashishta, P., Gwanmesia, G., Wang, Y. and Liebermann, R. C., "Intermediate-Range Order in Permanently Densified Vitreous SiO_2: A Neutron-Diffraction and Molecular-Dynamics Study," Physical Review B, 43, 1, 1991, 1194.

[34] Yu, J., Sinnott, S. B. and Phillpot, S. R., "Charge Optimized Many-Body Potential for the Si/SiO_2 System," Physical Review B, 75, 8, 2007, 085311.

[35] Plimpton, S., "Fast Parallel Algorithms for Short-Range Molecular Dynamics," Journal of Computational Physics, 117, 1, 1995, 1-19.

[36] Shan, T. -R., Devine, B. D., Hawkins, J. M., Asthagiri, A., Phillpot, S. R. and Sinnott, S. B., "Second-Generation Charge-Optimized Many-

Body Potential for Si/SiO_2 and Amorphous Silica," Physical Review B, 82, 23, 2010, 235302.

[37] Mukherjee, G. D., Vaidya, S. N. and Sugandhi, V., "Direct Observation of Amorphous to Amorphous Apparently First-Order Phase Transition in Fused Quartz," Physical Review Letters, 87, 19, 2001, 195501.

[38] Mozzi, R. L. and Warren, B. E., "The Structure of Vitreous Silica," Journal of Applied Crystallography, 2, 4, 1969, 164-172.

[39] Levita, G., Kajita, S. and Righi, M. C., "Water Adsorption on Diamond (111) Surfaces: An Ab Initio Study," Carbon, 127, 2018, 533-540.

[40] Petrini, D. and Larsson, K., "Theoretical Study of the Thermodynamic and Kinetic Aspects of Terminated (111) Diamond Surfaces," The Journal of Physical Chemistry C, 112, 8, 2008, 3018-3026.

[41] Sque, S. J., Jones, R. and Briddon, P. R., "Structure, Electronics, and Interaction of Hydrogen and Oxygen on Diamond Surfaces," Physical Review B, 73, 8, 2006, 085313.

[42] Kern, G., Hafner, J. and Kresse, G., "Atomic and Electronic Structure of Diamond (111) Surfaces I. Reconstruction and Hydrogen-Induced De-Reconstruction of the One Dangling-Bond Surface," Surface Science, 366, 3, 1996, 445-463.

[43] Feldbauer, G., Wolloch, M., Bedolla, P. O., Redinger, J., Vernes, A. and Mohn, P., "Suppression of Material Transfer at Contacting Surfaces: The Effect of Adsorbates on Al/Tin and Cu/Diamond Interfaces from First-Principles Calculations," Journal of Physics: Condensed Matter, 30, 10, 2018, 105001.

[44] Lowell, J. and Truscott, W. S., "Triboelectrification of Identical Insulators. I. An Experimental Investigation," Journal of Physics D: Applied Physics, 19, 7, 1986, 1273.

[45] Lowell, J., "Mechanisms of Contact Charging and Charge Accumulation: Experiments on Soda Glass," Journal of Physics D: Applied Physics, 24, 3, 1991, 375.

[46] Lowell, J., "Contact Electrification of Silica and Soda Glass," Journal of Physics D: Applied Physics, 23, 8, 1990, 1082.

[47] Lacks, D. J. and Mohan Sankaran, R., "Contact Electrification of Insulating Materials," Journal of Physics D: Applied Physics, 44, 45, 2011, 453001.

[48] Harper, W. R., "Contact and Frictional Electrification," Clarendon Press, 1967.

[49] Shaw, P. E., "Experiments on Tribo-Electricity. I. The Tribo-Electric Series," Proceedings of the Royal Society of London A: Mathematical, Physical and Engineering Sciences, 94, 656, 1917, 16-33.

[50] Dickinson, J. T., Scudiero, L., Yasuda, K., Kim, M. -W. and Langford, S. C., "Dynamic Tribological Probes: Particle Emission Andtransient Electrical Measurements," Tribology Letters, 3, 1, 1997, 53-67.

[51] Momose, Y., Yamashita, Y. and Honma, M., "Observation of Real Metal Surfaces by Tribostimulated Electron Emission and Its Relationship to the Analyses by XPS and Photoemission," Tribology Letters, 29, 1, 2008, 75-84.

[52] Molina, G. J., Furey, M. J., Ritter, A. L. and Kajdas, C., "Triboemission from Alumina, Single Crystal Sapphire, and Aluminum," Wear, 249, 3-4, 2001, 214-219.

[53] Mazilu, D. A. and Ritter, A., "The Abrasive Wear of Alumina: Correlation with Electron Triboemission," Wear, 258, 9, 2005, 1384-1403.

[54] Kornfeld, M. I., "Frictional Electrification," Journal of Physics D: Applied Physics, 9, 8, 1976, 1183.

[55] Nakayama, K., "Tribocharging and Friction in Insulators in Ambient Air," Wear, 194, 1-2, 1996, 185-189.

[56] Baytekin, H. T., Patashinski, A. Z., Branicki, M., Baytekin, B., Soh, S. and Grzybowski, B. A., "The Mosaic of Surface Charge in Contact Electrification," Science, 333, 6040, 2011, 308-312.

[57] Singer, I. L., Dvorak, S. D., Wahl, K. J. and Scharf, T. W., "Role of Third Bodies in Friction and Wear of Protective Coatings," Journal of Vacuum Science & Technology A, 21, 5, 2003, S232-S240.

[58] Tang, W., Sanville, E. and Henkelman, G., "A Grid-Based Bader Analysis Algorithm without Lattice Bias," Journal of Physics: Condensed Matter, 21, 8, 2009, 084204.

[59] Henkelman, G., Arnaldsson, A. and Jónsson, H., "A Fast and Robust Algorithm for Bader Decomposition of Charge Density," Computational Materials Science, 36, 3, 2006, 354-360.